# Gas Phase Spectroscopic Studies of Hydroquinone Dimer

**N. Biswas, S. Chakraborty, and S. Wategaonkar***

*Department of Chemical Sciences, Tata Institute of Fundamental Research, Homi Bhabha Road, Colaba, Mumbai 400005, India*

*Received: July 5, 2004; In Final Form: August 13, 2004*

Hydroquinone is one of the molecules that forms organic inclusion compounds, which have a wide range of commercial and technological applications. A lot of work has been done on this important molecule in the solid phase, but so far no work has been reported on its homoclusters in the gas phase. We report here the spectroscopic study of the hydroquinone dimer carried out under the jet-cooled conditions using the resonantly enhanced multiphoton ionization (REMPI) technique. The REMPI spectrum was quite rich in terms of the low-frequency transitions indicative of substantial geometry change upon excitation. The number of possible conformers formed in the jet was identified using the hole-burning spectroscopy. Ab initio calculations at the Hartree−Fock, density functional theory level using B3LYP functional and MP2 level for the ground state and the CIS level for the first excited state were carried out to understand the Franck−Condon activity in the spectrum as well as the number of possible stable conformers.

## Introduction

In last two decades, spectroscopic as well as dynamics studies of weakly bound complexes have become an actively pursued area of research in chemical physics. This has mainly been due to the ability of forming such complexes using the supersonic jet expansion and probing them using a variety of mass selective spectroscopic techniques. The typical issues that are addressed are solvation,[1] reaction dynamics,[2] intramolecular phenomena[3] such as intramolecular vibrational redistribution (IVR) or vibrational predissociation at low energies, H-bonded structures,[4] catalysis,[5] and so forth. The common motivation behind such studies is to acquire microscopic information about the weak interactions between the molecules which eventually may lead to a better understanding of the bulk phenomena. The typical problems addressed are the following: What is the smallest number of molecules needed before the gaseous cluster of molecules displays a condensed phaselike behavior? What are the types of intermolecular forces that pack the substance in a particular crystal structure? The latter question is apparently of great significance in the context of "crystal engineering",[6,7] aimed at designing novel supramolecular assemblies and crystalline structures with desired properties.

In this work, we report the spectroscopic studies on hydroquinone (HQ) homogeneous complexes. HQ is a crystalline solid at room temperature with a very high melting point (173 °C). This is not surprising because it has the ability to form a large H-bonding network as a result of the existence of the two OH groups in the para position. In the solid phase, this molecular system has been studied in great detail due to its ability to form clathrates, a type of organic inclusion compound.[8] Solid HQ is known to exist in three different polymorphs.[9] Out of these three, $\beta$-hydroquinone forms a cagelike structure[10] (clathrate host structure) which is a property desirable for the organic inclusion compounds. To date, however, no data is available for its homoclusters in the gas phase. The spectroscopy of HQ monomer[11] has been reported earlier, and it has been shown that HQ exists as trans and cis isomers in the gas phase. The water complex of HQ[12] has also been studied, and it has been reported that both isomers form the water complex with similar propensity. Therefore, a priori, at least four H-bonded conformers of the dimer could be anticipated, in addition to several other T-type or sandwich structures. However, only two distinct conformers were identified using the hole-burning (HB) spectroscopy.

There have been reports in the literature about the homodimers of phenol[13−16] and its derivatives.[17] In the case of dimer the two monomer moieties are bound to each other by means of H bonding similar to the phenol−water complex, except that one of the monomers acts as the proton donor and the other acts as an acceptor. However, unlike the resonantly enhanced multiphoton ionization (REMPI) spectrum of its water complex, the spectrum of the homodimer is marked by richness in regard to the low-frequency transitions that appear in progressions. This indicates a large change in the equilibrium geometry of the complex upon the electronic excitation. We have carried out extensive ab initio calculations at the Hartree−Fock (HF), density functional theory (DFT), and MP2 levels for the $S_0$ state and the CIS calculation for the excited state to understand the spectral features in the dimer spectrum. In addition, we have been able to identify a number of different stable equilibrium structures of the hydroquinone dimer (HQD) at these levels of calculations for the ground state.

## Experimental Details

The experimental setup consisted of two 10-in. diameter differentially pumped stainless steel chambers separated by a 2-mm skimmer. A 500-$\mu$m pulsed nozzle (General valve, series 9) opened into one chamber, and the skimmed molecular beam was taken into the second chamber, which housed the time-of-flight mass spectrometer (TOFMS). The TOFMS was of the Wiley−McLaren design[19] with a 0.5-m flight tube. The ions were extracted by pulsed electric fields using high voltage fast transistor switches (Behlke Electronics, Germany) and detected using a 10-mm channeltron (Phillips X919AL). The output of the channeltron was sent to a digitizing storage oscilloscope (Lecroy 9450).

10.1021/jp0470501 CCC: $27.50 © 2004 American Chemical Society
Published on Web 09/23/2004

For REMPI experiments, a 10-Hz nanosecond $Nd^{3+}$:YAG laser (Quantel YG781C) was used to pump two dye lasers (Quantel TDL70 and Molectron DL18P) to provide the tunable $S_0-S_1$ excitation and $S_1-D_0$ ionization beams, respectively. The excitation laser was scanned from 288 to 302 nm using the frequency doubled output of two sets of dyes, namely, R610+R640 and R590+R610 (Exciton, Inc.). The line width of the Quantel dye laser was 0.08 $cm^{-1}$ and that of the Molectron was 0.3 $cm^{-1}$. Care was taken so that the total two-photon energy was just sufficient to ionize the clusters or slightly higher to prevent fragmentation. The excitation and the ionization laser beams were spatially and temporally overlapped. The typical pulse energies were ~100 $\mu$J for the excitation laser and ~1 mJ for the ionization laser.

For the HB spectroscopy,[20] the YG781C YAG pumped TDL70 dye laser was used as the pump laser to scan the $S_0-S_1$ transitions, while the Quantel Brilliant YAG/Molectron DL18P dye laser combination was used as the probe beam. The probe beam was electronically delayed with respect to the pump beam by 250−300 ns. The typical pulse energies for the probe and the pump were ~100 $\mu$J and ~1 mJ, respectively. The problem of slow detector recovery following its saturation due to the huge ion flux generated by the pump beam was eliminated by using a special pulse sequence for the extraction grids.

HQ is a solid at room temperature and was heated to ~150 °C to generate enough vapor pressure to record spectra with a reasonable S/N ratio. HQ was purchased from S.D. Fine Chemicals, Ltd., and used without further purification. The helium buffer gas was from the local commercial sources and was used without further purification. The typical stagnation pressure was 1 atm. The typical working pressure in the source chamber was ~$1 \times 10^{-4}$ Torr, and in the TOFMS chamber it was ~$1 \times 10^{-6}$ Torr.

## Computational Details

To get more insight into the experimental results, the optimized structures and vibrational modes of the ground electronic state ($S_0$) were calculated using ab initio methods at the HF, DFT (with B3LYP functional), and post HF MP2 levels using the 6-31G* basis set. These calculations were carried out using the Gaussian 98 package.[21] To obtain all possible stable structures corresponding to various local minima initially semiempirical calculations were done to save time and effort. A number of configurations were generated, and each of such configurations was optimized semiempirically using the PM3 Hamiltonian. This was accomplished using a small program[22] developed using the Chemical Developer's Kit of the HyperChem (version 5.11) suite.[23] The few configurations on which the semiempirical calculations converged were then subjected to the ab initio calculations. No symmetry restrictions were applied during geometry optimization. In addition, the CIS (for the first excited state) calculations were also carried out for the two lowest energy conformers, vide infra.

The geometries of the optimized structures obtained from the ab initio calculations are presented with respect to the Cartesian coordinate system centered on the donor moiety of the complex (Figure 1). The center of mass (c.m.) of the donor moiety was placed at the origin with its aromatic ring coplanar with the $x-y$ plane and the CO bonds along the $x$ axis. The distance $\mathbf{R}_{\mathbf{c.m.}}$ depicts the c.m. distance between the two monomers, and $\Theta_{c.m.}$ and $\Phi_{c.m.}$ give the angles made by the $\mathbf{R}_{\mathbf{c.m.}}$ vector with the $z$ axis and the projection of $\mathbf{R}_{\mathbf{c.m.}}$ in the $x-y$ plane with the $x$ axis, respectively. The other angles (not shown in the figure), namely, the angle made by the $z'$ axis (of the coordinate system centered on the acceptor moiety after translating its origin to the reference origin) with the $z$ axis and that by the $x'$ axis with the $x$ axis (after aligning the $z'$ axis with the $z$ axis) are defined as $\theta_{zz'}$ and $\phi_{xx'}$, respectively. The $\theta_{zz'}$ gives the dihedral angle between the two aromatic rings. The binding energies (BEs) and the intermolecular vibrational modes of the optimized H-bonded conformers of the dimers were also calculated and are presented in the results section.

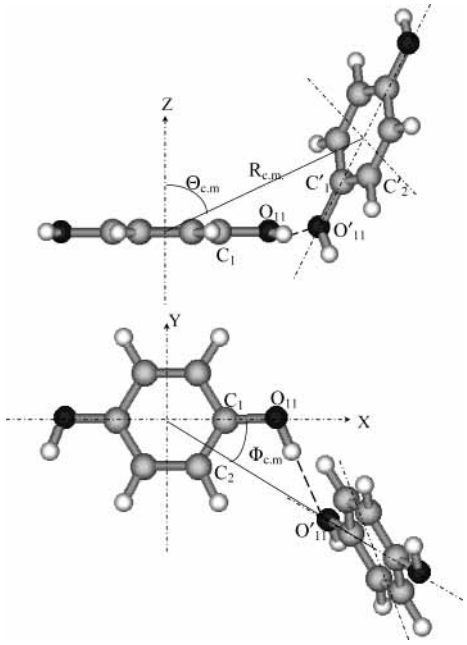


**Figure 1.** Definition of various geometrical parameters describing the relative positions of the constituent monomers in the H-bond donor-fixed reference Cartesian coordinate system.

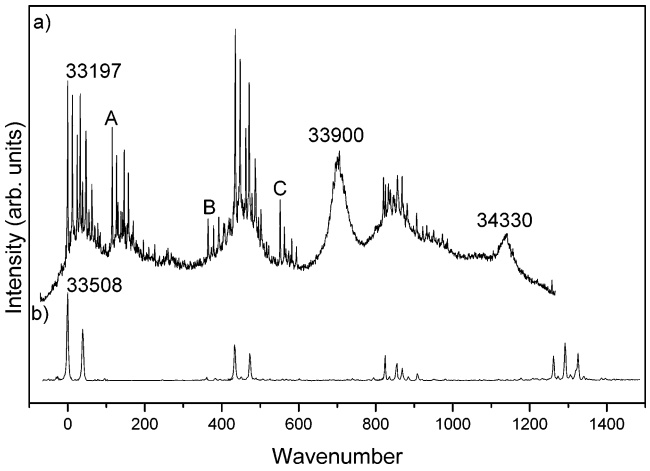


**Figure 2.** Two-color two-photon REMPI spectrum of (a) HQD and (b) HQ monomer recorded under the following expansion conditions. Stagnation pressure = 1 atm He; nozzle diameter = 500 $\mu$m; nozzle temperature = 150 °C. The ionization laser energy was set at 31 486 $cm^{-1}$. Spectra a and b are corrected for the laser power. The lowest energy transitions of the dimer that is, 33 197 $cm^{-1}$, and that of the monomer at 33 508 $cm^{-1}$ are aligned as the zero of the $x$ axis for better comparison of the two spectra.

## Experimental Results

Figure 2a shows the two-color two-photon REMPI spectrum of HQD where mass 220 au was monitored. The spectrum was quite rich in regard to the number of low-frequency transitions and comprised of clusters of such transitions superimposed on top of a small broad continuum. The lowest energy transition

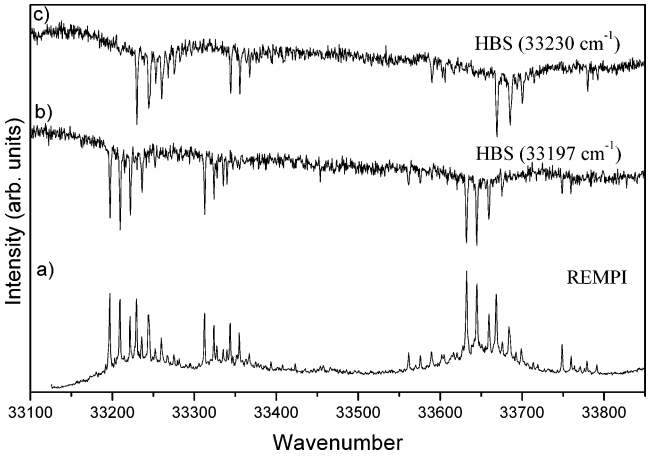


**Figure 3.** HB spectra of HQD in the BO region. Trace a is the REMPI spectrum, trace b is the HB spectrum probed for the 33 197 $cm^{-1}$ transition, and trace c is the HB spectrum with probe at the 33 230 $cm^{-1}$.

was observed at 33 197 $cm^{-1}$. Figure 2b shows the REMPI spectrum of HQ monomer. In the figure, the lowest energy transitions of the monomer (33 508 $cm^{-1}$) and the dimer (33 197 $cm^{-1}$) are aligned as the zero of the energy scale to facilitate the comparison. The HQ monomer spectrum mainly consists of a progression in the 6a mode and combinations of 6a with other totally symmetric modes, namely, 1 and 7a. It is also seen that band origin (BO) as well as every other transition appears in a pair, because of the presence of both trans and cis isomers in the jet. The separation between the BOs of the two isomers was 39 $cm^{-1}$, where the lower energy one corresponded to that of the trans isomer.[11] The dimer spectrum (Figure 2a) shows some resemblance with that of the monomer; that is, the clusters of peaks appeared at the positions exactly where the mode 6a and mode 1 transitions appear in the monomer spectrum. In addition, the similar pattern of the cluster transitions appeared with their onset at the energy spacing of 116, 364, and 552 $cm^{-1}$ (marked as A, B, and C in Figure 2a) from the lowest energy transition at 33 197 $cm^{-1}$. Besides the discrete transitions two broad peaks were observed centered at ~33 900 and 34 330 $cm^{-1}$. Apparently there are no analogous transitions in the REMPI spectrum of the monomer.

In the case of weakly bound complexes such as the dimer, the REMPI spectrum consists of transitions due to the low-frequency intermolecular vibrations, and in addition there is a possibility of transitions due to various distinct conformers. Because HQ monomer exists as trans and cis isomers, in the HQD one expects at least four different H-bonded structures, namely, the trans(donor)−trans(acceptor), trans(donor)−cis-(acceptor), cis(donor)−cis(acceptor), and cis(donor)-trans-(acceptor), in addition to perhaps other less stable sandwich/T-shaped structures. To identify the number of different conformers present in the jet each transition in the neighborhood of the 33 197 $cm^{-1}$ feature in the REMPI spectrum was probed using HB spectroscopy. Figure 3b,c shows the representative HB spectra for the 33 197 and 33 230 $cm^{-1}$ excitations. The HB spectra clearly show only two mutually exclusive sets of transitions indicating the presence of only two distinct isomers. The lowest energy transitions, namely, 33 197 and 33 230 $cm^{-1}$, were assigned to the BOs of the two conformers of HQD. The separation between the two BOs was 33 $cm^{-1}$.

All observed transitions are tabulated in Table 1 as two different sets corresponding to the two conformers, that is, one set with its origin at 33 197 $cm^{-1}$ (conformer A) and the other at 33 230 $cm^{-1}$ (conformer B). The entire spectrum can be

**TABLE 1: Observed Transitions in the REMPI Spectrum of HQD and Their Assignments**

| $\Delta E$ ($cm^{-1}$ with respect to the BO at 33 197 $cm^{-1}$) | assignment | $\Delta E$ ($cm^{-1}$ with respect to the BO at 33 230 $cm^{-1}$) | assignment |
|---|---|---|---|
| 0 | BO | 0 | BO |
| 12 | BO + $12^1$ | 15 | BO + $15^1$ |
| 24 | BO + $12^2$ | 23 | BO + 23 |
| 39 | BO + 24 + $15^1$ | 30 | BO + $15^2$ |
| 55 | BO + 24 + $15^2$ | 38 | BO + 23 + $15^1$ |
| | | 45 | BO + $15^3$ |
| | | 52 | BO + 23 + $15^2$ |
| | | 60 | BO + $15^4$ |
| | | 67 | BO + 23 + $15^3$ |
| 116 | H-bond stretch ($\sigma$) | 114 | H-bond stretch ($\sigma$) |
| 128 | $\sigma + 11^1$ | 126 | $\sigma + 11^1$ |
| 131 | $\sigma + 15$ | 138 | $\sigma + 11^2$ |
| 139 | $\sigma + 11^2$ | 149 | $\sigma + 11^3$ |
| 143 | $\sigma + 15 + 12^1$ | 163 | $\sigma + 49$ |
| 150 | $\sigma + 11^3$ | 178 | $\sigma + 49 + 15^1$ |
| 155 | $\sigma + 15 + 12^2$ | 193 | $\sigma + 49 + 15^2$ |
| 364 | $16a^2$ | 360 | $16a^2$ |
| 379 | $16a^2 + 15^1$ | 375 | $16a^2 + 15^1$ |
| 394 | $16a^2 + 15^2$ | 390 | $16a^2 + 15^2$ |
| 435 | $6a^1$ | 438 | $6a^1$ |
| 448 | $6a^1 + 12^1$ | 454 | $6a^1 + 15^1$ |
| 463 | $6a^1 + 12^1 + 15^1$ | 462 | $6a^1 + 23$ |
| 479 | $6a^1 + 12^1 + 15^2$ | 469 | $6a^1 + 15^2$ |
| | | 477 | $6a^1 + 23 + 15^1$ |
| | | 484 | $6a^1 + 15^3$ |
| 552 | $6a^1 + \sigma$ | 549 | $6a^1 + \sigma$ |
| 563 | $6a^1 + \sigma + 12^1$ | 561 | $6a^1 + \sigma + 12^1$ |
| 567 | $6a^1 + \sigma + 15^1$ | | |
| 574 | $6a^1 + \sigma + 12^2$ | | |
| 579 | $6a^1 + \sigma + 15^2$ | | |
| 820 | $1^1$ | 823 | $1^1$ |
| 825 | X | 836 | $9b^2$ |
| 833 | $1^1 + 12^1$ | 847 | $1^1 + 23$ |
| 838 | $9b^2$ | 873 | $6a^2$ |
| 845 | $1^1 + 12^2$ | 889 | $6a^2 + 15$ |
| 847 | $1^1 + 12 + 15$ | | |
| 850 | $9b^2 + 12$ | | |
| 859 | $1^1 + 12^2 + 15$ | | |
| 869 | $6a^2$ | | |
| 882 | $6a^2 + 12$ | | |
| 898 | $6a^2 + 12 + 15$ | | |
| 933 | $1^1 + \sigma$ | | |

explained as the progressions, vide infra, of the low-frequency intermolecular modes in combination with (1) an intermolecular mode at 116 (114) $cm^{-1}$, (2) the intramolecular 6a mode at 435 (438) $cm^{-1}$, (3) the combination band of the 6a and the intermolecular mode at 552 (549) $cm^{-1}$, and (4) the ring breathing mode 1 at 820 (823) $cm^{-1}$, where the numbers in parentheses refer to conformer B. In addition, a small progression also appeared in combination with the intramolecular $16a^2$ mode at 364 (360) $cm^{-1}$.

Figure 4 shows an expanded view of the REMPI spectrum in the BO region. The transitions due to each of the conformers are separated with the help of the HB spectrum for the sake of clarity. The REMPI spectra of conformer A (Figure 4a) and conformer B (Figure 4b) show many interesting features. The observed progressions are indicated by the markers indicating the spacing between the successive members in $cm^{-1}$. A four-member progression was observed on the BO conformer A. The spacing between the first two members was ~12 $cm^{-1}$ whereas that between the next two was ~15 $cm^{-1}$. For conformer B, a four member progression with an equal spacing of 15 $cm^{-1}$ was observed on the BO as well as on a transition at 23 $cm^{-1}$ from

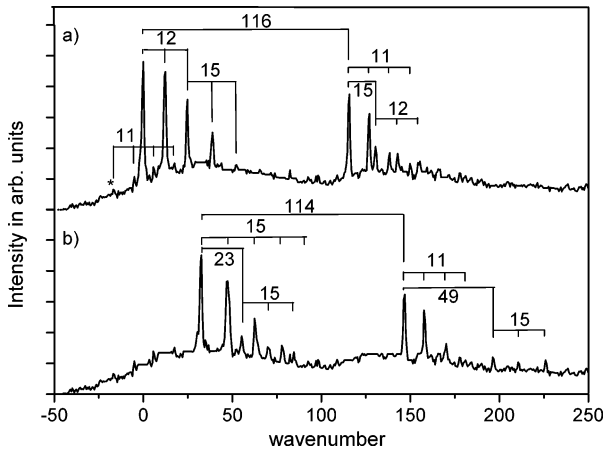


**Figure 4.** Expanded region of the REMPI spectrum of the dimer near the BO. The transitions due to the two conformers are separated with the help of the HB spectrum. The horizontal scales with numbers indicate various progressions, indicating the spacing between the successive members. The transition marked with an asterisk is the hot band.

the BO. The absence of the 23 $cm^{-1}$ transition in conformer A and the irregular spacing between the members of the observed progression can be explained if it is assumed that the transition corresponding to the 23 $cm^{-1}$ transition in conformer B is overlapped by the 24 $cm^{-1}$ transition (second member of the 12 $cm^{-1}$ progression) and the next two members are actually the members of the 15 $cm^{-1}$ progression based on this overlapped transition. Thus, for conformer A three vibrational modes, that is, 12, 15, and 24 $cm^{-1}$, were observed. For conformer B only one progression was observed with a 15 $cm^{-1}$ spacing on the BO and on a 23 $cm^{-1}$ mode. Apart from these low-frequency modes a strong transition (almost as strong as the BO) was observed at 116 $cm^{-1}$ from the BO of conformer A and at 114 $cm^{-1}$ from that of conformer B. The low-frequency progressions were also observed in combination with these two transitions, but the pattern of the progressions for the two conformers was completely different from that observed for the respective BOs. For conformer A two progressions were observed; one with 11 $cm^{-1}$ spacing on the BO and the other with 12 $cm^{-1}$ spacing in combination with a transition at 15 $cm^{-1}$ from the 116 $cm^{-1}$ transition. For the other conformer only the 11 $cm^{-1}$ progression was observed (this progression was not observed in conjunction with its BO for this conformer). A weak transition was also observed at 49 $cm^{-1}$ with a weak progression of 15 $cm^{-1}$ based on it. A weak progression with the spacing of 11 $cm^{-1}$ was also observed based on a transition at 16 $cm^{-1}$ (marked by an asterisk in the figure) to the red side of the lowest energy BO. The 16 $cm^{-1}$ transition was assigned to a hot band on the basis of the intensity dependence on the expansion conditions.

## Computational Results

The HF and DFT calculations converged to four stable geometry-optimized H-bonded structures (I−IV as shown in Figure 5) in addition to three T-type structures (V−VII), one sandwich-type structure (VIII), and one coplanar structure (IX; Figure 5S, Supporting Information). To get a rough estimate of the stability order of these conformers, the BEs for all the optimized structures were calculated at the HF level. For weakly bound complexes, although the HF/6-31G* level calculation does not give reliable BEs, it does a fair job of giving the relative stabilities and is much faster. For the four most stable H-bonded conformers (structures I−IV) the BEs were further refined using

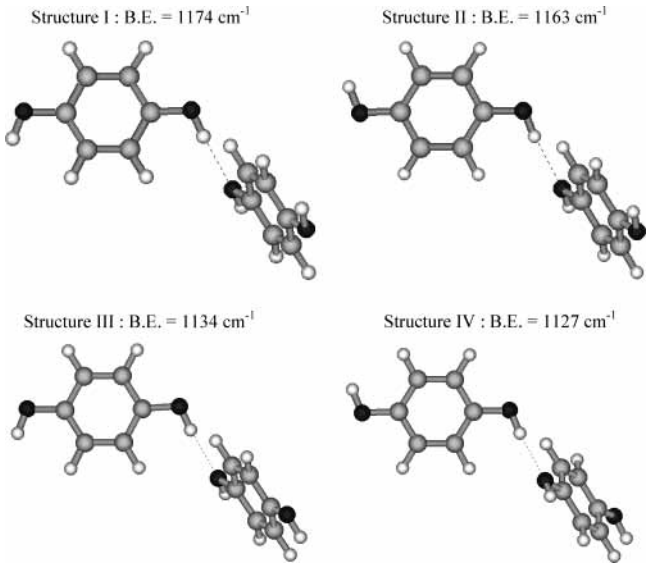


**Figure 5.** H-bonded structures of the HQD optimized at the HF level using the 6-31G* basis set. The number for the each structure indicates its BE (see text and Table 2 for further details).

**TABLE 2: BEs in $cm^{-1}$ Corrected for the BSSE (Counterpoise Method) and the ΔZPE and the Deformation Energy (DE) for the Four H-bonded Conformers Calculated at the HF and MP2 Levels Using the 6-31G* Basis Set**

| | structure I | | structure II | | structure III | | structure IV | |
|---|---|---|---|---|---|---|---|---|
| | HF | MP2 | HF | MP2 | HF | MP2 | HF | MP2 |
| BE | 1174 | 1649 | 1163 | 1643 | 1134 | 1600 | 1127 | 1591 |
| BSSE | 489 | 1390 | 499 | 1384 | 480 | 1363 | 492 | 1370 |
| ΔZPE | 360 | 381 | 363 | 373 | 349 | 360 | 354 | 359 |
| DE | 72 | 72 | 67 | 73 | 69 | 72 | 64 | 71 |

the post-HF method, vide infra. The coplanar structure was the most weakly bound structure (BE = 175 $cm^{-1}$), followed by the T-type structure (VII; BE = 263 $cm^{-1}$). For the other two T-type structures and the sandwich-type structure the BE was in the 400−500 $cm^{-1}$ range. All these structures, however, were considerably weaker compared to the H-bonded structures (I−IV). The HF BEs of the H-bonded structures were 1174, 1163, 1134, and 1127 $cm^{-1}$, respectively. These were inclusive of the basis set superposition error (BSSE)[24] and the zero point energy difference (ΔZPE), as well as the deformation energy (the energy difference between the isolated equilibrium geometry of the monomer and the geometry of the monomer in the complex), the details of which are given in Table 2. The ΔZPE for all of them was roughly the same, that is, ∼360 $cm^{-1}$, which is about ∼23% of the BE. The cis(d)−trans(a) dimer (structure I, Figure 5) was found to be the most stable, followed by the trans−trans dimer (structure II) which was less stable by 11 $cm^{-1}$. The trans(d)−cis(a) and the cis−cis pairs (III and IV) were less stable by ∼40 $cm^{-1}$ compared to the most stable structure.

It is known that although HF or DFT calculations do not recover the full electron correlation energies, the geometry is predicted very well at these levels, at least for the cases that do not include the van der Waals interactions. However, in the case of phenol dimer for which extensive experimental data exist,[13,16] it was found that the HF/DFT structures did not agree well with the experiments but the MP2 calculations at the 6-31G* level did an excellent job.[16] This suggests that both electrostatic and dispersive interactions are at play in these cases. In the present case also we carried out the MP2 level calculation using 6-31G* basis set for all four H-bonded conformers. Their BEs for the

**TABLE 3: Geometric Parameters for the cis(d)−trans(a) [Structure I] and trans(d)−trans(a) [Structure II] H-Bonded Dimers Optimized Using the 6-31G* Basis Set at the MP2, HF, and DFT(B3LYP) Levels for the $S_0$ State and at the CIS Level for the $S_1$ State[a]**

| | calculation level | | | | | | | |
|---|---|---|---|---|---|---|---|---|
| | MP2 | | HF | | DFT | | CIS | |
| parameters | I | II | I | II | I | II | I | II |
| $\mathbf{R}_{c.m.}$ | 5.534 | 5.576 | 6.682 | 6.711 | 6.572 | 6.587 | 6.402 | 6.410 |
| $\angle\Theta_{c.m.}$ | 56.3 | 57.8 | 67.8 | 68.8 | 66.1 | 66.6 | 63.3 | 63.7 |
| $\angle\Phi_{c.m.}$ | 46.5 | 46.8 | 31.7 | 31.6 | 29.2 | 29.3 | 36.7 | 37.3 |
| $\angle\theta_{zz}'$ | 73.3 | 74.1 | 73.7 | 72.2 | 70.6 | 69.9 | 77.3 | 75.7 |
| $\angle\phi_{xx}'$ | 47.2 | 52.9 | 28.7 | 27.8 | 17.3 | 17.7 | 62.3 | 64.7 |
| $\angle C_1-O_{11}-O_{11}'-C_1'$ | 67.7 | 68.8 | 107.5 | 109.4 | 110.8 | 111.3 | 87.6 | 86.7 |
| $\angle C_2-C_1-O_{11}-O_{11}'$ | −9.1 | −7.5 | −2.4 | −1.4 | −4.4 | −4.0 | −7.3 | −7.2 |
| $\angle C_2'-C_1'-O_{11}'-O_{11}$ | −14.4 | −14.3 | 3.2 | 3.4 | 6.2 | 5.7 | 36.2 | 36.7 |
| ∠linear deviation of the H bond | 15.5 | 14.8 | 10.8 | 10.6 | 12.2 | 12.2 | 7.0 | 6.7 |
| $O_{11}-O_{11}'$ | 2.874 | 2.871 | 2.952 | 2.952 | 2.859 | 2.857 | 2.904 | 2.902 |
| H-bond length | 1.919 | 1.913 | 2.013 | 2.012 | 1.897 | 1.894 | 1.954 | 1.952 |
| $C_1-O_{11}$(donor) | 1.374 | 1.374 | 1.353 | 1.354 | 1.369 | 1.369 | 1.322 | 1.323 |
| $C_1'-O_{11}'$(acceptor) | 1.390 | 1.390 | 1.368 | 1.368 | 1.388 | 1.387 | 1.370 | 1.370 |
| $O_{11}-H$(donor) | 0.979 | 0.980 | 0.951 | 0.951 | 0.977 | 0.977 | 0.955 | 0.955 |
| $O_{11}'-H$(acceptor) | 0.974 | 0.974 | 0.948 | 0.947 | 0.969 | 0.969 | 0.948 | 0.948 |

[a] All the distances are in angstroms, and the angles are in degrees.

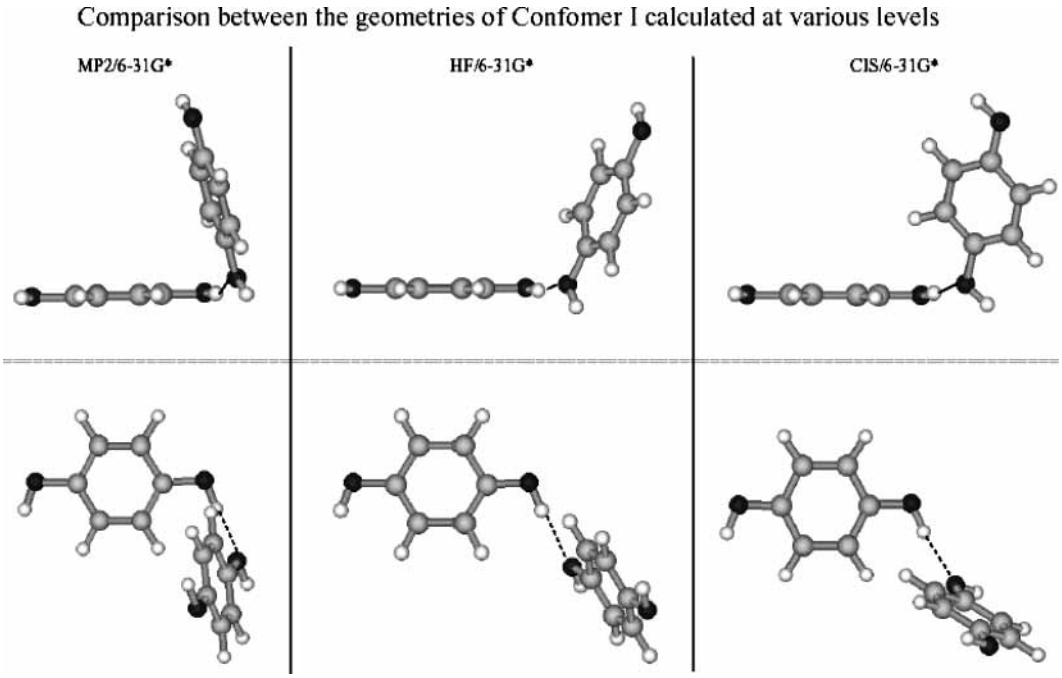


**Figure 6.** Side view (top row) and the top view (bottom row) of the HQD equilibrium structure I calculated at the MP2, HF, and CIS levels.

structures I−IV improved to 1649, 1643, 1600, and 1591 $cm^{-1}$, respectively (see Table 2 for details). The BSSE corrections even at this level are of the order of ∼1390 $cm^{-1}$, which are quite large. It has been shown in the case of the analogous phenol dimer[17] that to obtain the best value of the BE, it was necessary to invoke basis sets with higher order polarization functions. However, such calculations are beyond our resources.

All the four conformers belong to the lowest $C_1$ symmetry group. For the sake of brevity the optimized structural parameters for only the two lowest energy conformers in the $S_0$ state at the HF/DFT/MP2 level and the $S_1$ state at the CIS level are given in Table 3. Figure 6 shows the side and the top view of the equilibrium structures calculated at the MP2, HF, and the CIS level for structure I to clearly bring out the differences graphically. By and large, both the structures were V-shaped with the intermolecular ($\mathbf{R}_{c.m.}$) distances of 6.682 (6.572) and 6.711 (6.587) Å, respectively, at the HF (DFT) level of calculations. At the MP2 level the $\mathbf{R}_{c.m.}$ distance decreased to 5.534 and 5.576 Å, respectively, for the two conformers. This decrease, however, is not along the H-bonding coordinate but due to the decrease in the dihedral angle $\angle C_1O_{11}-O_{11}'C_1'$ from ∼108 to ∼68°. In other words in the equilibrium structure calculated at the MP2 level the acceptor ring folds back onto the donor ring thereby bringing the two c.m.'s closer to each other. With the result the angle $\Theta_{c.m.}$ also decreased from ∼68 to ∼56°. The H-bond length and the O−O distance for structure I at the HF (DFT) level were 2.013 (1.897) and 2.952 (2.859) Å, respectively, as opposed to 1.919 and 2.874 at the MP2 level indicating very little change in the geometry along this coordinate. The hydrogen bonds in both the conformers deviate from linearity by 10−12° out of the donor plane and the acceptor oxygen atom ($O_{11}'$) is shifted out of the plane ($\angle C_2C_1O_{11}O_{11}'$) by about −1 to −2° (HF) and −4.0 to −4.4° (DFT). These deviations were larger for the MP2 level calculations. The dihedral angle between the acceptor aromatic plane and the plane containing the H bond, that is, $\angle C_2'C_1'O_{11}'O_{11}$, was 3−6° in

the case of HF and DFT structures; however, this increased to ~14° in the case MP2 level calculated structures.

The intramolecular OH distances for the donor and acceptor counterparts were 0.951 and 0.948 Å for the structure I and 0.951 and 0.948 Å for the structure II, respectively. The bond distances for the nonparticipating OH oscillators were between 0.947 and 0.948 Å for both the structures. This is consistent with the fact that the proton donating O−H bond that participates in the H bonding suffers elongation. This is also reflected in the intramolecular O−H stretching frequencies. The vibrational frequencies scaled by a factor of 0.9 for the donor and acceptor moieties were 3648 ± 1 and 3706 ± 1 $cm^{-1}$ for both the structures, respectively. The C−O bond distances for the moiety acting as a H donor varied from 1.353 to 1.354 Å (HF) and 1.369 Å (DFT), and for the one acting as the H-acceptor, it was around 1.368 Å (HF) and 1.387−1.388 Å (DFT). At the MP2 level also this trend was confirmed, and the CO bond distances were in better agreement with the DFT numbers than with the HF numbers. The C−O bond lengths of the HQ monomer (cis and trans monomers have similar C−O bond lengths) as obtained from HF and DFT were 1.358 and 1.373 Å, respectively. This indicates that, in the dimer, the C−O bond distance of the acceptor moiety increases and that in the donor decreases slightly compared to the monomer. Also the increase for the acceptor is much larger compared to the decrease in the donor. This is consistent with the increased charge density on the O atom in the donor as expected in the H-bonded species.

Table 3 also gives the geometrical parameters for the excited state calculated at the CIS level. In Figure 6 the equilibrium structure in the excited state is compared with those for the ground state (MP2/HF) to bring out the dramatic change upon excitation. It is quite instructive to note the changes in the key parameters. In the following, the CIS values are compared with only the HF values because it will be inappropriate to compare with the MP2 values. For example, the torsional angle ($\angle C_1O_{11}O_{11}C_1$) changes from 107.5 to 87.6° (side view in Figure 6), and the dihedral angle between the acceptor ring and the plane containing the H bond changes from 3.2 to 36.2° (top view). Similar changes also take place in the case of structure II (also see Table 3). The changes in these two angles were quite large and certainly reflect in the appearance of the REMPI spectrum, vide infra. The $\mathbf{R}_{c.m.}$ distance decreases from 6.682 to 6.402 Å. The donor O−H bond elongates to 0.955 Å from 0.951 Å in the $S_0$ state consistent with the fact that the substituted phenols are much stronger acids in the excited state, which causes substantial strengthening of the H bond and weakening of the intramolecular OH bond in the donor moiety in the excited state.

Six intermolecular normal coordinates are required to fully characterize the dimer. These intermolecular coordinates are usually observed as the low-frequency vibrations ($\nu_1-\nu_6$) of the dimer. For all the structures, these intermolecular vibrational frequencies were calculated and were nonnegative (at all levels of calculations), confirming that all the structures indeed correspond to local minima and not to saddle points. For the most stable structure (I), the frequencies calculated at the HF/6-31G* level were 9, 23, 24, 51, 53, and 106 $cm^{-1}$ and those from the DFT/6-31G* calculations were 12, 28, 30, 55, 64, and 122 $cm^{-1}$. The vibrational frequencies for the other structures (II−IV) were within 1 or 2 $cm^{-1}$ of those of structure I. These frequencies were assigned to the butterfly or torsion ($\nu_1$), out-of-plane rocking or cogwheel motion ($\nu_2$), in-plane rocking ($\nu_3$), in-plane bend ($\nu_4$), out-of-plane bend ($\nu_5$), and H-bond stretching ($\nu_6$) modes in the increasing order of energy. For the most stable conformer the frequencies were also computed for the excited state. These were 17, 22, 30, 61, 66, and 111 $cm^{-1}$, respectively. For the H-bonded complexes it has been shown[25] that the large amplitude low-frequency intermolecular modes ($\nu_1-\nu_3$ in this case) that are derived from the rotational motion of the fragments are highly anharmonic in nature and their frequencies could in general be quite different (lower) than those computed based on the quadratic potentials used in the calculations. Further, because the equilibrium structures in both the $S_0$ as well as $S_1$ states belong to the $C_1$ point group there are no symmetry restrictions for any of the low-frequency intermolecular vibronic transitions.

## Discussion

The two conformers of HQD are 33 $cm^{-1}$ apart, whereas in the monomer, the separation between the trans and cis isomers was 39 $cm^{-1}$, with the trans isomer being lower in energy. The character of the REMPI spectrum is also quite similar to that of the monomer in regard to the pairwise appearance of each transition. If one draws a one-to-one correspondence, then the lowest energy BO can be assigned to a $\pi-\pi^*$ transition centered on the *trans*-HQ and the other one to the *cis*-HQ species involved in the dimer. The red shifts with respect to HQ are 311 and 317 $cm^{-1}$ for the two conformers of HQD, respectively. This magnitude of the red shift in the BO transitions is typical of the H-bonded complexes of phenol and its derivatives. In all these cases the phenol acts as a proton donor. Therefore, we assign the two observed conformers to the two most stable H-bonded structures calculated at the HF/DFT/MP2 level, namely, the cis(d)−trans(a) and trans(d)−trans(a) pairs (structures I and II, respectively). Further, the lowest energy transition at 33 197 $cm^{-1}$ (conformer A) was assigned to the trans(d)−trans(a), that is, structure II, and the 33 230 $cm^{-1}$ transition (conformer B) was assigned to the cis(d)−trans(a), that is, structure I, on the basis of the relative intensities (peak heights as well as peak areas) of the two BO transitions. It is known that for the monomer the trans isomer is more stable in the ground state relative to the cis isomer.[26] Therefore, the relative population of the trans monomer will be higher in the jet than that of the cis monomer no matter at which point during the expansion they freeze. Therefore, on the basis of simple stoichiometric arguments it can be shown that the number density of the trans(d)−trans(a) conformer ought to be higher in the jet than that of the cis(d)−trans(a) conformer.

It is known from the previous studies on the phenol dimer[13−16] that in such homodimers the two monomer units are no longer equivalent; that is, one of them is the proton donor and the other one is the proton acceptor. The donor BO is typically red shifted by ~300 $cm^{-1}$, and the acceptor BO is blue shifted by about the same amount. In the present context the broad feature observed at ~33 900 $cm^{-1}$ is blue shifted from the monomer BO by ~390 $cm^{-1}$ and there is no other analogous transition in the monomer spectrum. Therefore, it has been attributed to the BO transition of the acceptor moiety. The separation between the maxima of the two broad features was 430 $cm^{-1}$. This matches exactly with the 6a frequency of the monomer as well as that of donor moiety in the dimer. Therefore, the 34 330 $cm^{-1}$ band was assigned to the 6a mode of this acceptor moiety. The lack of structure in these two features may be due to other photophysical processes such as IVR, intersystem crossing, or internal conversion. Similar observations have also been reported in the case of *p*-cresol dimer.[18]

The dimer formation does not affect the intramolecular modes of the donor moiety significantly. In HQ monomer, the 6a[1]

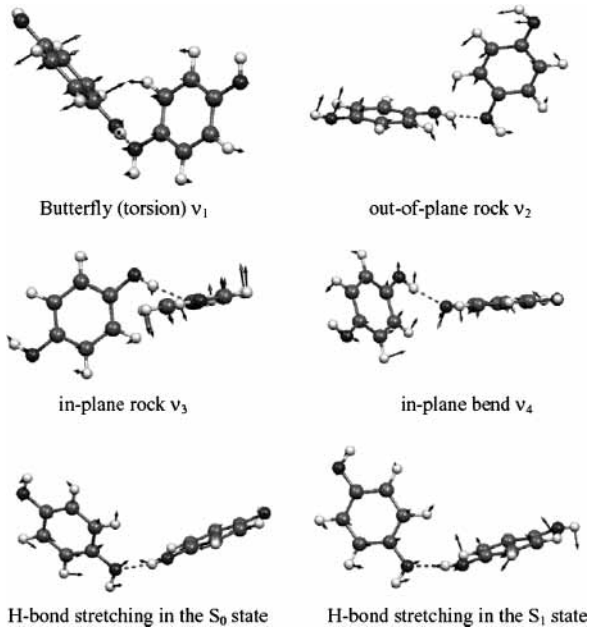


**Figure 7.** Normal mode descriptions for the $S_1$ excited state; also given is the H-bonding stretching mode description for the $S_0$ state.

vibrations of the trans and cis conformers appear at 441 and 440 $cm^{-1}$, respectively, while in the dimer these were observed at 435 $cm^{-1}$ for the conformer A and 438 $cm^{-1}$ for the other one. Also the mode 1 frequencies in the monomer were 824 and 826 $cm^{-1}$ for the trans and cis, respectively, whereas in the dimer these were 820 and 823 $cm^{-1}$. Apart from these two intramolecular transitions for conformer A the intermolecular modes were observed at 11, 12, 15, 24, and 116 $cm^{-1}$ whereas for conformer B the observed modes were at 11, 15, 23, 49, and 114 $cm^{-1}$.

The 12 and 15 $cm^{-1}$ modes appeared in progressions on the BOs as well as in combination with the intramolecular 6a and 16a modes and the H-bonding stretching mode for conformer A whereas for conformer B only the 15 $cm^{-1}$ progression was observed. In addition, an 11 $cm^{-1}$ progression was observed for both the conformers only in combination with the 116/114 $cm^{-1}$ transition. The appearance of strong progressions in the REMPI spectrum indicates a large change in the geometry along the corresponding normal modes. Figure 7 shows the first four intermolecular normal modes for the $S_1$ state of one of the conformers. It can be seen that the $\nu_1$ normal mode samples the geometry along the dihedral $\angle C_1O_{11}-O_{11}C_1$ whereas the $\nu_3$ normal mode is along the dihedral $\angle C_2'C_1'O_{11}'O_{11}$. As mentioned earlier, the equilibrium geometry in the $S_1$ state undergoes a large change in these two angles. Hence, we assign the observed 12 and 15 $cm^{-1}$ progressions to $\nu_1$ and $\nu_3$, respectively. These assignments are based purely on the comparison of computed normal modes with the changes in the geometry upon excitation relative to the $S_0$ state rather than any numerical agreement between the computed normal modes and the observed transitions. The 116/114 $cm^{-1}$ transitions were assigned to the H-bonding stretching frequency for the two conformers on the basis of the calculations. For the excited state the largest frequency for the intermolecular modes was computed as 111 $cm^{-1}$ and its mode description indicated that it is indeed the H-bond stretching mode (Figure 7). Interestingly, although the H-bond length decreased in the excited state from 2.013 to 1.954 Å (the HF vs CIS values) the stretching modes computed for the $S_0$ (106 $cm^{-1}$) and the $S_1$ states (111 $cm^{-1}$) are quite comparable to each other contrary to the observations (both theoretical and experimental) in the case of H-bonded complexes of phenols or their derivatives.[4] Phenol and its derivatives become strong acids in the excited state, and, hence, the H-bonding strength in the excited state is relatively much stronger than that in the ground state. As a the result, the H-bond stretching frequency blue shifts significantly in the excited state. In the present context, although the H-bond length change is consistent with the relative strength of the H-bond, the stretching frequency is not. This apparent anomaly can be reconciled if one takes into account the stretching normal mode description in the $S_0$ as well as the $S_1$ states as shown in Figure 7. It can be seen that in the $S_1$ state certain ring carbon atoms on the donor moiety have a significant out-of-plane amplitude as opposed to that in the $S_0$ state. This indicates that this mode is severely mixed with a low-frequency ring deformation mode located on the donor ring. Because the electronic excitation to the $S_1$ state involves a $\pi-\pi^*$ transition in the donor moiety, the $\pi$-bond order of the donor ring decreases considerably. During the H-bond stretching vibration due to the bulky acceptor moiety, the donor ring may suffer out-of-plane deformation along the low-frequency intramolecular ring deformation mode. This may explain why the stretching frequency in the excited state does not show as much blue shift as is in other cases, because it is no longer a pure mode.

The pattern of the low-frequency progressions observed in combination with the H-bond stretching mode was distinctly different than that based on the BO and other intramolecular modes. For example, an 11 $cm^{-1}$ progression was observed only in combination with the H-bonding stretching mode. There could be two possibilities. First, the 11 $cm^{-1}$ is another intermolecular mode that is Franck−Condon active only in combination with the stretching mode. The other is that there is a strong anharmonic coupling between the 12 $cm^{-1}$ mode and the stretching mode with the result that whenever it appears in combination with the stretching mode its frequency separation is 11 $cm^{-1}$. The second possibility is much more likely because the 11 $cm^{-1}$ progression is not observed anywhere else in the entire spectrum except in combination with the H-bond stretching mode.

Finally, it is interesting to note that the V-shaped structure of the dimer in the gas phase is similar to that observed in the solid phase. In the case of $\beta$-hydroquinone clathrate, stacks of six-membered H-bonded O−H···O rings form cagelike structures. The six HQ molecules are oriented alternately above and below the plane of the ring, forming the top and bottom of the cage due to the V shape of the dimer in which a guest molecule gets trapped. In the jet-cooled beam the higher members of the HQ clusters were observed up to $HQ_4$; however, their respective REMPI spectra were a broad band continuum void of any sharp features. This is an obvious result because there are a number of ways a third monomer and fourth monomer could attach to $HQ_2$ and $HQ_3$, respectively giving rise to helical or sheetlike structures analogous to the $\alpha,\gamma$-hydroquinone clathrates, leading to a congestion in the REMPI spectrum.

## Conclusions

HQD was studied in the jet-cooled molecular beam using two-color two-photon REMPI spectroscopy. With HB spectroscopy, only two distinct conformers were identified with BOs at 33 197 and 33 230 $cm^{-1}$. These have been assigned to the trans−trans and cis(d)−trans(a) configurations, respectively, on the basis of ab initio calculations at the HF, DFT(B3LYP), and MP2 levels using the 6-31G* basis set. The observed discrete transitions, the onset of which was red shifted by 311 (317) $cm^{-1}$ relative to the monomer BO transitions, were assigned to

the donor moieties of the respective conformer. The broad band transition observed in HQD shifted by 390 $cm^{-1}$ to the blue side of the HQ monomer was attributed to the BO of the acceptor moiety; discrete transitions due to the corresponding acceptor moiety were not observed. The BO transitions of the two dimers were accompanied by progressions in several low-frequency intermolecular bending modes. The H-bonding stretching vibrations of HQD were observed at ~115 $cm^{-1}$ in both conformers. These observations were in close agreement with those reported for the phenol dimer and *p*-cresol dimer.

**Supporting Information Available:** Figure depicting the structures V−XI of the dimer calculated at the HF/6-31G* level with the relevant geometrical parameters. This material is available free of charge via the Internet at http://pubs.acs.org.

## References and Notes

(1) (a) Zwier, T. S. *Annu. Rev. Phys. Chem.* **1996**, *47*, 205. (b) Leutwyler, S.; Bosiger, J. *Chem. Rev*. **1990**, *90*, 489. (c) Amirav, A.; Even, U.; Jortner, J. *J. Chem. Phys*. **1981**, *75*, 2489.

(2) (a) Castleman, A. W., Jr.; Wei, S. *Annu. Rev. Phys. Chem*. **1994**, *45*, 685. (b) Castleman, A. W., Jr.; Bowen, K. H., Jr. *J. Phys. Chem*. **1996**, *100*, 12911. (c) Shang, Q. Y.; Bernstein, E. R. *Chem. Rev*. **1994**, *94*, 2015.

(3) (a) Bernstein, E. R. *Annu. Rev. Phys. Chem*. **1995**, *46*, 197. (b) Nesbitt, D. J. *Annu. Rev. Phys. Chem*. **1994**, *45*, 367.

(4) (a) Ebata, T.; Fujii, A.; Mikami, N. *Int. Rev. Phys. Chem*. **1998**, *17*, 331. (b) Garrett, A. W.; Zwier, T. S.; Severance, D. L. *J. Phys. Chem*. **1992**, *96*, 9710. (c) Janzen, Ch.; Spangenberg, D.; Roth, W.; Kleinermanns, K. *J. Chem. Phys*. **1999**, *110*, 9898. (d) Palmer, P. M.; Topp, M. R. *Chem. Phys. Lett*. **1998**, *292*, 307. (e) Leutwyler, S.; Burgi, T.; Schutz, M.; Tylor, A. *Faraday Discuss.* **1994**, *97*, 1.

(5) Castleman, A. W., Jr.; Keesee, R. G. *Annu. Rev. Phys. Chem*. **1986**, *37*, 525.

(6) Desiraju, G. R. *Angew. Chem., Int. Ed. Engl*. **1995**, *34*, 2311.

(7) Müller, A.; Reuter, H.; Dillinger, S. *Angew. Chem., Int. Ed. Engl*. **1995**, *34*, 2328.

(8) *Inclusion compounds*; Atwood, J. L., Davies, J. E. D., MacNicol, D. D., Eds.; Academic: London, 1984; Vols. 1−3.

(9) Evans, D. F.; Richards, R. E. *J. Chem. Soc*. **1952**, *1952*, 3932.

(10) Hermansson, K. *J. Chem. Phys*. **2000**, *112*, 835.

(11) Patwari, G. N.; Doraiswamy, S.; Wategaonkar, S. *Chem. Phys. Lett*. **1998**, *289*, 8.

(12) Meenakshi, P. S.; Biswas, N.; Wategaonkar, S. *Phys. Chem. Chem. Phys*. **2003**, *5*, 294.

(13) Connell, L. L.; Ohline, S. M.; Joireman, P. W.; Corcoran, T. C.; Felker, P. M. *J. Chem. Phys*. **1992**, *96*, 2585.

(14) Dopfer, O.; Lembach, G.; Wright, T. G.; Müller-Dethlefs, K. *J. Chem. Phys.* **1993**, *98*, 1933.

(15) Schmitt, M.; Henrichs, U.; Müller, H.; Kleinermanns, K. *J. Chem. Phys*. **1995**, *103*, 9918.

(16) Weichert, A.; Riehn, C.; Brutschy, B. *J. Phys. Chem. A* **2001**, *105*, 5679.

(17) Hobza, P.; Riehn, A.; Weichert, B.; Brutschy, B. *Chem. Phys*. **2002**, *283*, 331.

(18) Yan, S.; Spangler, L. H. *J. Phys. Chem*. **1991**, *95*, 3915.

(19) Wiley, W. C.; McLaren, I. H. *Rev. Sci. Instrum*. **1955**, *26*, 1150.

(20) Lipert, R. J.; Colson, S. D. *J. Phys. Chem*. **1989**, *93*, 3894.

(21) Frisch, M. J., et al. *Gaussian 98*, revision A.11.2; Gaussian, Inc.: Pittsburgh, PA, 2002.

(22) Subashini, S. Project Report for Visiting Students Research Program. Tata Institute of Fundamental Research: Mumbai, India, 2001.

(23) *HyperChem, Molecular Modeling System*, Release 5.11 Pro for Windows; Hypercube, Inc.: Gainesville, FL, 1999.

(24) Boys, S. F.; Bernardi, F. *Mol. Phys.* **1970**, *19*, 553.

(25) Schütz, M.; Bürgi, T.; Leutwyler, S. *J. Chem. Phys*. **1993**, *98*, 3763.

(26) Humphrey, S. J.; Pratt, D. W. *J. Chem. Phys*. **1986**, *99*, 5078.